Supercapacitor Modeling and Parameter Identification of a 400 kW Grid-Connected Supercapacitor Energy Storage System using the Inherent Impedance Spectroscopy Capability of its DC/DC Converter

1st Michael Hetzel
Elektrotechnisches Institut (ETI)
Karlsruhe Institute of Technology (KIT)
Karlsruhe, Germany
michael.hetzel@kit.edu

2st Daniel Diaz Ocampo
Institut für Indust. Informationstechnik (IIIT)
Karlsruhe Institute of Technology (KIT)
Karlsruhe, Germany
daniel.diaz-ocampo@kit.edu

3rd Giovanni De Carne
Institut für Technische Physik (ITEP)
Karlsruhe Institute of Technology (KIT)
Karlsruhe, Germany
giovanni.carne@kit.edu

4st Marc Hiller
Elektrotechnisches Institut (ETI)
Karlsruhe Institute of Technology (KIT)
Karlsruhe, Germany
marc.hiller@kit.edu

Abstract—In this work, a 400 kW supercapacitor energy storage system (SCESS) with grid-serving converter for the 400 V grid is presented. A modeling approach for the supercapacitor energy storage (SCES) is presented and a method of parameter estimation using the inherent impedance spectroscopy capability of the SCESSs DC/DC converter is introduced. We determine the impedance of the SCES and investigate the suitability of the modeling approach. The results indicate that the proposed modeling and parameter identification method is suitable to model the voltage of the real SCES.

Index Terms—supercapacitor, modeling, parameter identification, impedance spectroscopy, energy storage system

I. INTRODUCTION

Grid-connected SCESSs can be utilized to provide grid services, such as smoothing renewable energy generation [1] or regulating grid frequency [2]. When doing so, they are often used in conjunction with other energy storage devices to increase energy capacity [3]. In common grid applications, the energy capacity of SCESSs mostly limits the possible operating scenarios. In order to use the limited energy of SCESSs in an optimal way, accurate modeling is required. This paper presents a method for modeling and identifying SCESs' electrical behaviour using solely the sensors of the DC/DC converter for the measurement, which accelerates commissioning and avoids the need for high-cost measurement equipment. In order to achieve this, the SCES is measured using an adapted form of impedance spectroscopy. In Section II, a 400 kW supercapacitor energy storage system (SCESS) with grid-serving converter for the 400 V grid is introduced. Section III describes a method to determine the frequency and voltage dependent impedance of an SCES using only the sensors of its DC/DC converter. In addition, the impedances of the test bench determined using the method are presented. Section IV presents a modeling approach for the electrical behavior of the SCES. In Section V, the parameter estimation of the model is described. Finally, in Section VI, the parameterized model of the test bench is presented and compared to the results of the impedance spectroscopy in the time and frequency domain.

II. PRESENTATION OF THE TEST BENCH

Fig. 1a depicts a schematic overview of the complete system, consisting of the grid connection, LCL-filter, active front end (AFE), three-phase DC/DC converter and the SCES itself. In Fig. 1b, a picture of the complete test bench is shown. The rated power of the entire system is 400 kW, the rated output current of the DC/DC converter is 1400 A. The switching frequency of the semiconductors of the DC/DC converter is 8 kHz. The SCES is designed with three parallel branches each consisting of 240 supercapacitors (SC) (*BCAP3000 P270*, Maxwell Technologies) connected in series. Each SC has a nominal capacitance of 3000 F and a rated voltage of 2.7 V. They are passively balanced via parallel resistors and actively balanced above a cell voltage of 2.5 V. The resulting capacitance of the SCES is 37.5 F with a maximum voltage of 600 V and a theoretical stored energy of 6.75 MWs. The test bench is controlled by a modular signal processing system based on the *ZYNQ7030* System-on-Chip (SoC) from *Xilinx* [4].
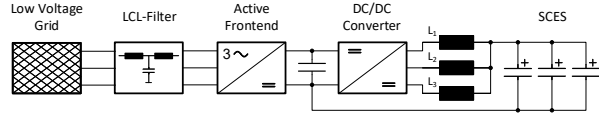
(a) System overview of the SCESS with converter, grid connection and the SCES.

(b) Image of the entire test bench.

Fig. 1: System overview of the SCESS and image of the entire test bench.

III. Impedance Spectroscopy

Impedance spectroscopy can be used to determine the impedance of a system as a function of frequency [5]. For this purpose, sinusoidal currents with different frequencies are injected into a system. The frequency dependant complex impedance $\underline{Z}$ is determined from the spectrum of the injected current and the resulting voltage. Usually this is done with a current amplitude in the milliamper range. If the impedance spectroscopy of a SCES is performed without additional hardware, a trade-off arises for the current amplitude to be injected. On the one hand, the current should be as large as possible to minimize the relative error of the current and voltage sensors. On the other hand, the voltage amplitude increases with the current amplitude, which in turn negatively affects the measurement due to the voltage dependence of the SCES. The current change in the chokes is limited by their possible voltage range and the dynamics of the current control. Here, the choke voltage depends on the voltage of the SCES, the DC link voltage and the dead time of the semiconductors. The maximum current change in the inductors in turn limits the maximum current amplitude and the maximum frequency. Finally, the impedance is determined as a function of the frequency and the DC voltage of the SCES. Due to the fact that SCESs have large time constants (in the range of weeks), the impedance measurements cannot be performed in steady state in practical applications. To minimize the influence of the large time constants, all measurement points should be performed at one voltage in succession. Measurement accuracy is further improved if measurements are made at a voltage from high to low frequency, because at measuring points with high frequency, the influence of the large time constants is smaller, whereas with lower frequencies the settling time is already larger. In addition, after a new voltage has been applied, the measurements should not be started directly.

A. Single measuring point determination

To determine the impedance $\underline{Z}$ of a single measuring point, the SCES is charged to the desired DC voltage. Then the sinusoidal current can be applied. It should be started with

a phase of 90° such that the mean value of the voltage deviates as little as possible from the desired value. The measurement of current and voltage should start when the sinusoidal current has already been applied for some time in order not to confound the measurement due to transient processes. The measurement point should persist over several complete periods to avoid spectral leakage and provide a sufficient spectral resolution. The amplitude and phase of voltage and current can be determined with the fast Fourier tranform. After transforming the voltage and current signals into the frequency domain, the maximum magnitude of each signal in the spectrum for frequencies greater than zero is examined. The impedance of the measuring point can then be determined and the frequency of the maximum then corresponds to:

$$f_{\text{sin}} = \frac{n}{N} \cdot f_{\text{sample}} \tag{1}$$

where n is the index of the maximum value, N is the number of elements of the FFT spectrum and f_{sample} is the sample rate of the measured values.

Since only one frequency value of the spectrum is considered for the calculation of the amplitude, broadband noise has a smaller effect at the results. Additionally, the more periods are measured, the higher is the frequency resolution, which results in a higher signal to noise ratio due to averaging.

B. Impedance determination of the SCES of the test bench

The impedance determination was performed for voltages from $100\,\text{V}$ to $500\,\text{V}$ in $50\,\text{V}$ steps and frequencies in the range from $12.5\,\text{mHz}$ to $400\,\text{Hz}$. The amplitude of the injected current was chosen so that a voltage change at the SCES of $10\,\text{V}$ was not significantly exceeded and the limits of the DC/DC converter voltage were not reached. In addition, the maximum current amplitude was limited to $200\,\text{A}$.

The absolute value, argument, real part and imaginary part of the determined impedance $\underline{Z}_{\text{meas}}$ are displayed in Fig. 2. From the figure it can be seen that the impedance is very dependent on the frequency. Compared to this, its voltage dependence is rather low. In the measured frequency range, the magnitude of $\underline{Z}_{\text{meas}}$ decreases with increasing frequency. The phase angle increases from -80 to just above zero degrees. The real part of $\underline{Z}_{\text{meas}}$ also decreases with increasing frequency. The imaginary part increases with the frequency and becomes positive for high frequencies.

If the impedance of a SCES is modeled as a serial RLC circuit the capacity is given by

$$C_{\text{SCES}} = \frac{1}{\omega^2 \cdot L_{\text{SCES}} - \omega \cdot Im(\underline{Z}_{\text{SCES}})} \tag{2}$$

and the resistance R is then equal to $R_{\text{SCES}} = Re(\underline{Z}_{\text{SCES}})$. The resulting capacitance for the SCES of the test bench with this approach is displayed in Fig. 3. Here, L_{SCES} was determined from the voltage swing within one pulse period to be $1.334\,\mu\text{H}$.

In the lower frequency range C_{SCES} has a voltage dependence, which decreases strongly above $0.2\,\text{Hz}$. In addition, the capacitance is nearly constant for low frequencies, and
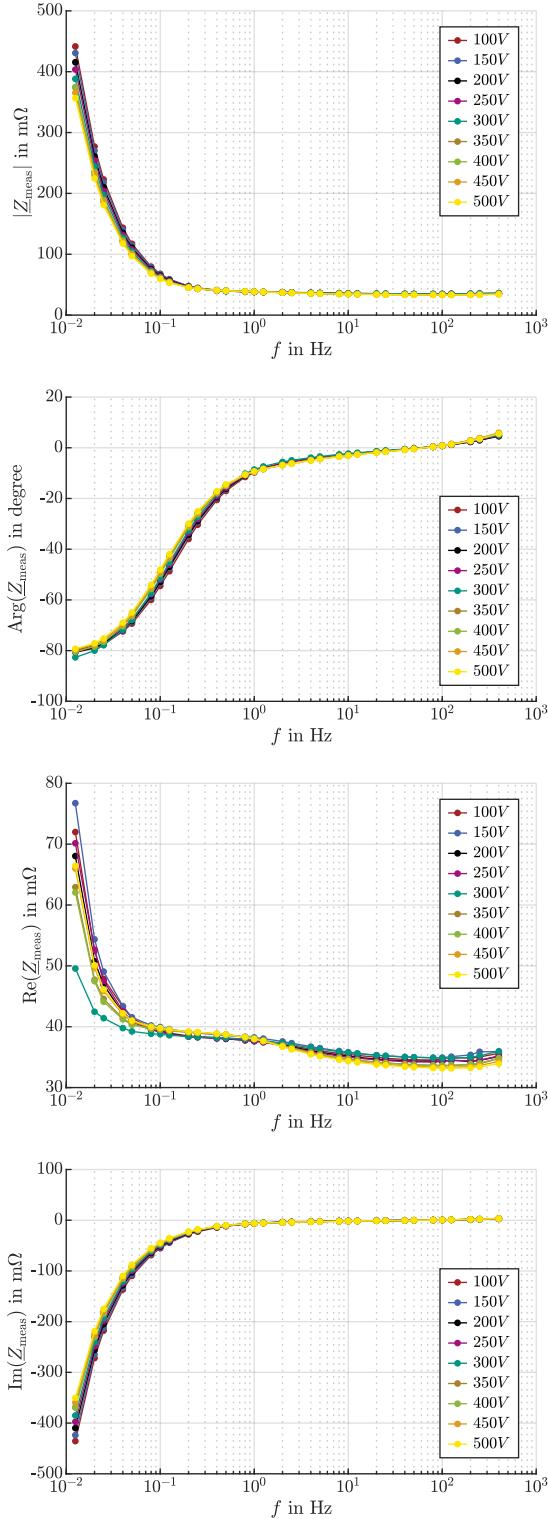
Fig. 2: Absolute value, argument, real and imaginary parts of the impedance of the SCES determined from the measurements for different voltages.
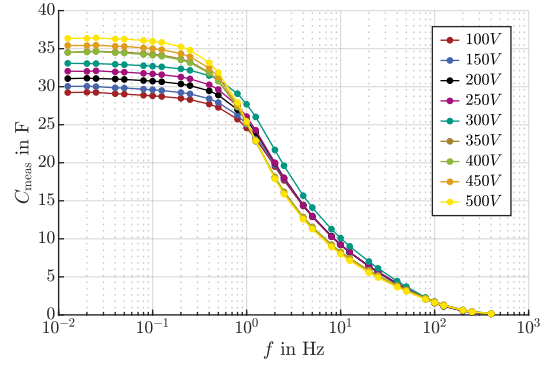
Fig. 3: The voltage and frequency dependent equivalent capacitance of the SCES determined from the measurements for different voltages.

decreases to nearly zero as the frequency increases. The resistance R_{SCES} first decreases sharply with increasing frequency, then forms a plateau, decreases further, and then slightly increases again from about $100\,\mathrm{Hz}$. It is obvious that the simple RLC model is not able to adequately represent the voltage and frequency dependent behavior of the SCES, which requires a more complex modeling of the electrical behavior.

IV. MODELING

A reliable model of SCESs is the basic requirement for their design and operation. The behavior of SCs differs significantly from the behavior of other types of capacitors and requires a different modeling approach. There are many different published models in the literature. [6] introduces an modeling approach for SCs. In [7], [8] and [9] a summary of basic modeling approaches of the electrical behavior of SCs are provided. In [10], different modeling approaches are combined into one model.

Most of these modeling approaches can be summarized with the equivalent circuit diagram in Fig. 4. The equivalent circuit consists of five parts:

1) A main RC element, which reflects the essential behavior of the SCES. It consists of a series connection of R_0 and C_0, where the capacitance usually corresponds to:

$$C_0(u_{\mathrm{C0}}) = C_{0,\mathrm{const}} + k \cdot u_{\mathrm{C0}} \qquad (3)$$

where u_{C0} is the voltage across C_0, $C_{0,const}$ is the capacitance C_0 at $u_{C0} = 0\,\mathrm{V}$, and k is the gain of the linear capacitance change of C_0 due to voltage u_{C0}.

2) Serial RC elements, which increase the resistance in the path of the main RC element for low frequencies.

3) Parallel RC elements, which represent slow transients and allow charge redistribution between the parallel elements.

4) A leakage resistor, which represents the self-discharge of the SCES and whose time constant is in the range of weeks.

5) An inductance L, which takes into account the inductive behavior of the SCES at high frequencies.
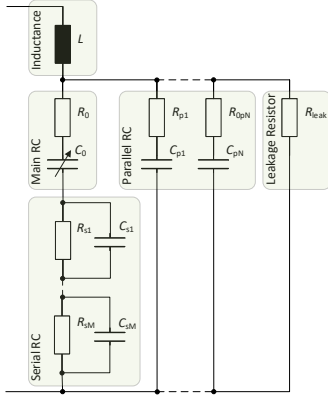
Fig. 4: Generalized SCES model.

Fig. 5: Models used for iterative SCES parameter identification.

This model is applied to SCESs operated as short-time energy storage systems with high pulse power. The model is used to determine the power dissipation and energy in addition to the terminal voltage and the state of charge. Since the application is for short-time energy storage system with high power, only the modeling of time intervals in the range of minutes is necessary. For this reason, the modeling of the leakage resistor can be neglected. Since the loss energy is also determined from the model, charging processes must be accurately modeled for higher frequencies. The final model used for this analysis consists of one inductor L, one main RC element, one serial and two parallel RC elements.

V. PARAMETER ESTIMATION

To fit the model to the SCESs behaviour, the model parameters must be estimated. Eq. 4 describes the impedance of the generalized model neglecting the leakage Resistor. Here, N and M are the number of parallel and serial RC elements.

$$\underline{Z}_{\mathrm{sMpN}} = \frac{1}{\sum_{n=0}^{N}\left(\frac{1}{\underline{Z}_{\mathrm{pn}}}\right)} + j\omega L \qquad (4)$$

where $\underline{Z}_{\mathrm{pn}}$ is the impedance of the parallel paths, defined as

$$\underline{Z}_{\mathrm{pn}} = \begin{cases} R_0 + \frac{1}{j\omega C_0} + \sum_{m=1}^{M}\left(\frac{R_{sm}}{j\omega C_{sm}R_{sm}+1}\right) & ,n=0 \\ R_{\mathrm{p}n} + \frac{1}{j\omega C_{\mathrm{p}n}} & ,n>0 \end{cases} \qquad (5)$$

The model parameters were estimated using Matlab's non-linear least squares solver *lsqnonlin*. The solver determines the model parameters by fitting the model impedance determinded from Eq. 4 to the impedances determined from the measured data. In addition to the determined parameters, the model impedance depends on the frequency f and the capacitor voltage u_{C0}. The inductance L was specified as a fixed value for the parameter estimation. Parameter estimation was performed iteratively. The identification was started with the main RC element. Then the serial element was added. Subsequently, the model was successively extended by the parallel elements. In this process, the parameters of the previous model serve as the starting value of the next one. The models for the individual

iteration steps are shown from left to right in Fig. 5, where each submodel MsMpN has M serial and N parallel RC elements. The resulting parameters of the estimated models are shown in Table I.
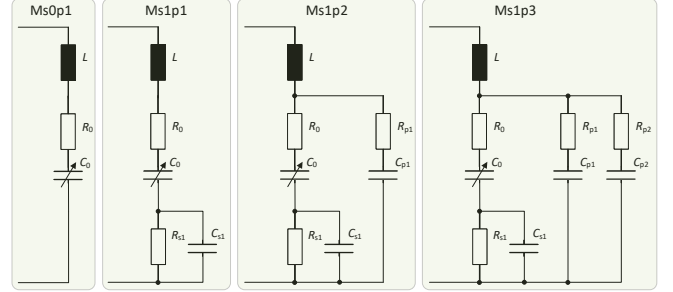
VI. RESULTS

In this section the impedances determined from the measurements are compared with those of the parameterized models in the frequency and time domain.

A. Frequency domain

Fig. 6 shows the impedance determined from the measurement, as well as that of the parameterized models for the SCES at $u_{\mathrm{SCES}} = 200\,\mathrm{V}$ in two frequency ranges. The overall characteristic looks quite similar for other voltages.

The general curve of the measured impedance of the SCES can be described as follows: as frequency increases, the imaginary part increases more than the real part up to about $0.5\,\mathrm{Hz}$. For further increasing frequencies, the imaginary part then approaches zero, with the real part dropping. For frequencies above about $40\,\mathrm{Hz}$, the real part remains nearly constant and the imaginary part increases and becomes positive. Ms0p1 represents a straight line in the complex plane and therefore cannot reasonably represent the course of the impedance of the SCES. With increasing model complexity, the models get closer to the impedance of the SCES. For very low frequencies, the real part of the SCES increases significantly. Only Ms1p2 and Ms1p3 have the same behavior, although they still show significant deviations compared to the SCES at very low frequencies. For high frequencies, only Ms1p2 and Ms1p3 are able to approximate the impedance response of the SCES.

In Fig. 7, the deviation between the models and the measurements for the real and imaginary parts of the impedance and the capacity for all meassured voltages are shown. It can be seen that voltage has an influence on the deviation of the models for the real and imaginary parts of the impedance, as well as the capacitance. The statements for Fig. 6 also apply to other voltages of the SCES. For the capacity of the models, the deviation decreases for higher frequencies with increasing model complexity, with a little difference between Ms1p2

TABLE I: Model parameters.

model	L in µF	k_0 in µF/V	R_0 in mΩ	$C_{0,\mathrm{const}}$ in F	$R_{\mathrm{p},1}$ in Ω	$C_{\mathrm{p},1}$ in F	$R_{\mathrm{p},2}$ in Ω	$C_{\mathrm{p},2}$ in F	$R_{\mathrm{s},1}$ in mΩ	$C_{\mathrm{s},1}$ in F
M_{s0p1}	1.334	18.532	39.169	26.942	-	-	-	-	-	-
M_{s1p1}	1.334	18.709	35.108	27.224	-	-	-	-	4.0436	20.495
M_{s1p2}	1.334	18.709	34.824	26.176	2.769	1.655	-	-	4.2661	12.284
M_{s1p3}	1.334	17.323	35.247	25.659	2.493	1.820	3.085	1.450	4.2717	11.673
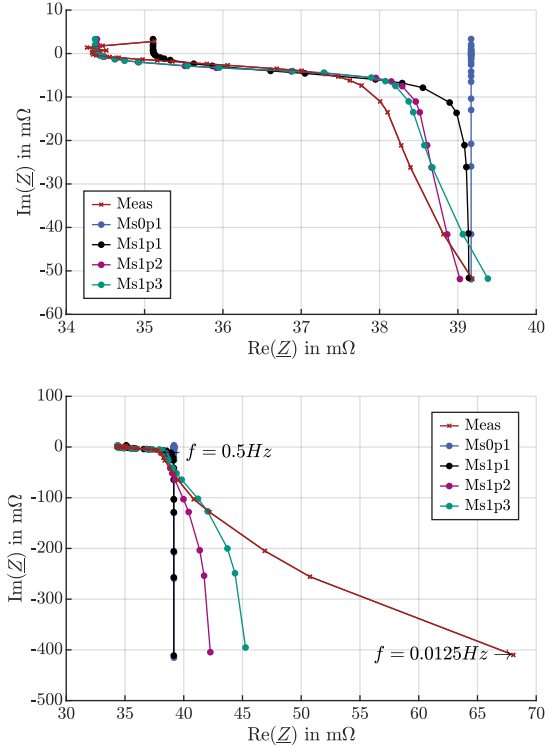
Fig. 6: Impedance of the SCES determined from measured values, as well as the impedance of the parameterized models in the complex plane at $u_{\mathrm{SCES}} = 200\,\mathrm{V}$. From $0.1\,\mathrm{Hz}$ to $400\,\mathrm{Hz}$ in (a) and $12.5\,\mathrm{mHz}$ to $400\,\mathrm{Hz}$ in (b).

and Ms1p3. The capacitance deviation increases at very low frequencies, with increasing model complexity. Ms1p2 and Ms1p3 also show minimal differences for frequencies above $0.2\,\mathrm{Hz}$ for the real and imaginary parts of the impedance. For all measured voltages and frequencies above $0.1\,\mathrm{Hz}$, Ms1p3 reduces the model error of the real part to a maximum of $5\,\mathrm{m\Omega}$ and that of the imaginary part to below $1\,\mathrm{m\Omega}$. The model error of the capacitance is below $4\,\mathrm{F}$ for all certain frequencies and voltages.

B. Time domain

The models are intended to model charging and discharging processes of the SCES. Therefore, the accuracy in the time domain is crucial for their application. In Fig. 8(a), the measured voltage and current curve of the SCES, as well as the voltage curve of the models Ms0p1, Ms1p1, Ms1p2 and Ms1p3 are shown for three charging cycles. The models

receive the measured current waveform of the SCES as input. The initial voltage of all parallel capacitors equals the initial terminal voltage of the SCES. The initial voltage of the serial capacitor is zero. The SCES is charged from $100\,\mathrm{V}$ to $540\,\mathrm{V}$ and then discharged again. There is a pause of $20\,\mathrm{s}$ between charging and discharging. The first charging cycle is done with a constant current of $500\,\mathrm{A}$ and increases with each cycle by $100\,\mathrm{A}$. Fig. 8(b) shows the voltage error of the models for the same charging cycles as in Fig. 8(a). It can be concluded that the model accuracy for all quantities increases significantly with increasing model complexity. This consideration also coincides with the representation of the model impedance in the complex domain in Fig. 6. It can also be seen that the change in the model error in the resting times and during the charging and discharging phases decreases with increasing model complexity. For M1s3, the deviation over the entire course of time is less than $0.5\,\%$ of the nominal voltage of the SCES.

VII. CONCLUSION

In this work, a method for modeling and parameter estimation of a $400\,\mathrm{kW}$ supercapacitor energy storage (SCES) is presented. It uses the inherent impedance spectroscopy capabilities of its DC/DC converter to determine the frequency and voltage dependent impedance of the SCES. This impedance is used to estimate the model parameters in the frequency domain. The results are then validated in the frequency domain by compairing the determined impedance with the impedance of the models. In addition, the models were validated in the time domain using constant current charging cycles. The results indicate that at least one serial and two parallel RC paths are needed to model the short-term behavior of the voltage sufficiently accurately. It can be concluded that the method we present is suitable for the identification of the model parameters. The parameterized model can serve as a starting point for an online identification of state of charge (SoC) or state of energy (SoE) of the SCES and can thereby increase its usable energy.

REFERENCES

[1] J. Pegueroles-Queralt, F. D. Bianchi, and O. Gomis-Bellmunt, "A power smoothing system based on supercapacitors for renewable distributed generation," *IEEE Transactions on Industrial Electronics*, vol. 62, no. 1, pp. 343–350, 2015.

[2] R. Zhang, J. Fang, and Y. Tang, "Inertia emulation through supercapacitor energy storage systems," in *2019 10th International Conference on Power Electronics and ECCE Asia (ICPE 2019 - ECCE Asia)*. IEEE, 2019.
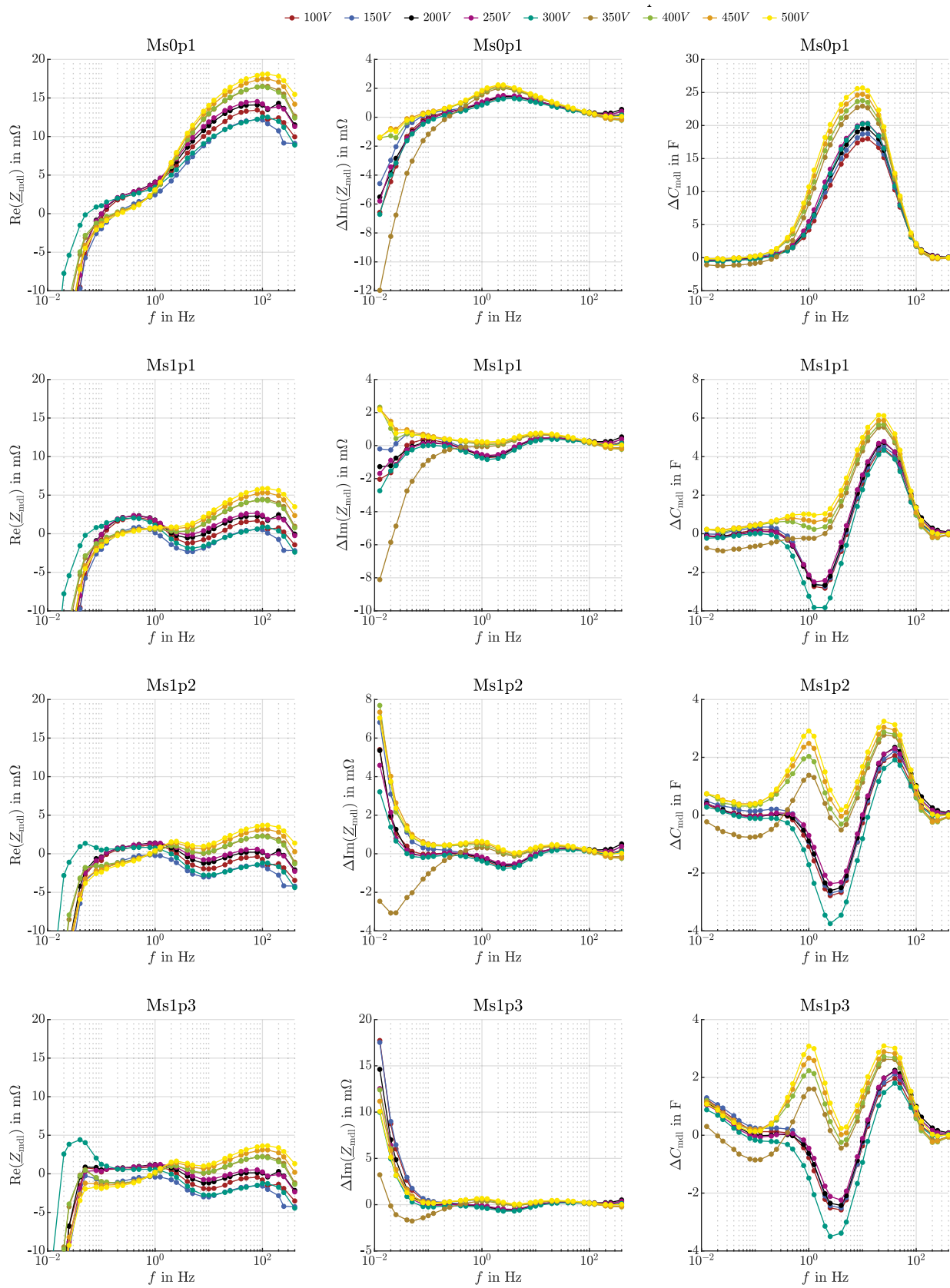
Fig. 7: Deviation between the models and measurement of the real an imaginary part of the impedance and the capacity as a function of frequency.
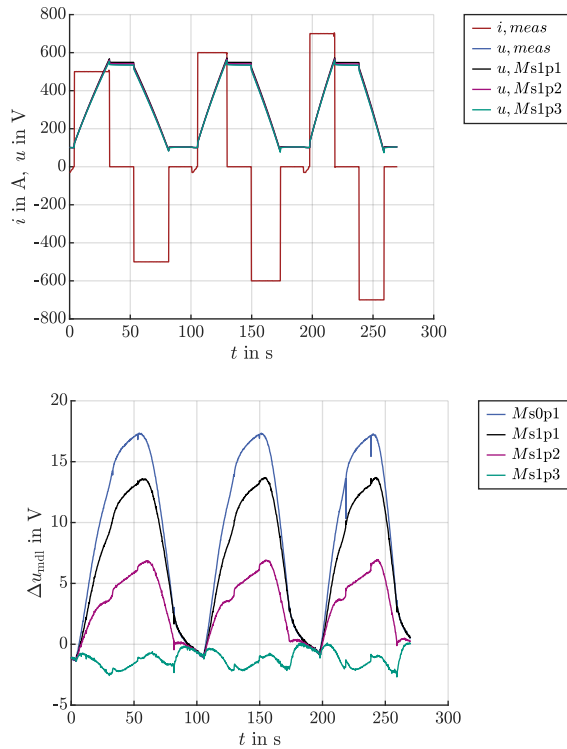
Fig. 8: In (a) the voltage and current of the SCES as well as its model voltage for three charging cycles with a constant current of 500 A, 600 A and 700 A are displayed. (b) shows the model deviation between the real SCES and the different models for the three charging cycles.

[3] Y. Kim, V. Raghunathan, and A. Raghunathan, "Design and management of battery-supercapacitor hybrid electrical energy storage systems for regulation services," *IEEE Transactions on Multi-Scale Computing Systems*, vol. 3, no. 1, pp. 12–24, 2017.

[4] B. Schmitz-Rode, L. Stefanski, R. Schwendemann, S. Decker, S. Mersche, P. Kiehnle, P. Himmelmann, A. Liske, and M. Hiller, "A modular signal processing platform for grid and motor control, hil and phil applications," in *2022 International Power Electronics Conference (IPEC-Himeji 2022- ECCE Asia)*. IEEE, uuuu-uuuu, pp. 1817–1824.

[5] V. F. Lvovich, *Impedance Spectroscopy: Applications to electrochemical and dielectric phenomena*. Hoboken, New Jersey: Wiley, 2012. [Online]. Available: https://ebookcentral.proquest.com/lib/kxp/detail.action?docID=817407

[6] L. Zubieta and R. Bonert, "Characterization of double-layer capacitors for power electronics applications," *IEEE Transactions on Industry Applications*, vol. 36, no. 1, pp. 199–205, 2000.

[7] A. Berrueta, A. Ursua, I. S. Martin, A. Eftekhari, and P. Sanchis, "Supercapacitors: Electrical characteristics, modeling, applications, and future trends," *IEEE Access*, vol. 7, pp. 50 869–50 896, 2019.

[8] M. Şahin, "Modelling of supercapacitors based on simplified equivalent circuit," *CPSS Transactions on Power Electronics and Applications*, vol. 6, no. 1, pp. 31–39, 2021.

[9] X. Chang, D. Lei, S. Zhang, S. Li, and Y. Yang, "Novel supercapacitor model parameter identification methods," in *2017 2nd International Conference on Power and Renewable Energy*, ICPRE, Ed. Piscataway, NJ: IEEE Press, 2017, pp. 81–86.

[10] A. Morandi, A. Lampasi, A. Cocchi, F. Gherdovich, U. Melaccio, P. L. Ribani, C. Rossi, and F. Soavi, "Characterization and model parameters of large commercial supercapacitor cells," *IEEE Access*, vol. 9, pp. 20 376–20 390, 2021.